
BYTESTORM: A MULTI-STEP DATA-DRIVEN APPROACH FOR TROPICAL CYCLONES DETECTION AND TRACKING

A PREPRINT

 **Davide Donno**^{1,2}

 **Donatello Elia**¹

 **Gabriele Accarino**^{1,3}

 **Marco De Carlo**¹

 **Enrico Scoccimarro**¹

 **Silvio Gualdi**¹

1 CMCC Foundation - Euro-Mediterranean Center on Climate Change, Via Marco Biagi, 5, Lecce, Italy

2 University of Salento, Department of Engineering for Innovation, Via per Monteroni, Lecce, Italy

3 Department of Earth and Environmental Engineering, Columbia University, New York, NY, USA

ABSTRACT

Accurate tropical cyclones (TCs) tracking represents a critical challenge in the context of weather and climate science. Traditional tracking schemes mainly rely on subjective thresholds, which may introduce biases in their skills on the geographical region of application. We present *ByteStorm*, an efficient data-driven framework for reconstructing TC tracks without threshold tuning. It leverages deep learning networks to detect TC centers (via classification and localization), using only relative vorticity (850 mb) and mean sea-level pressure. Then, detected centers are linked into TC tracks through the BYTE algorithm. *ByteStorm* is evaluated against state-of-the-art deterministic trackers in the East- and West-North Pacific basins (ENP and WNP). The proposed framework achieves superior performance in terms of Probability of Detection (85.05% ENP, 79.48% WNP), False Alarm Rate (23.26% ENP, 16.14% WNP), and high Inter-Annual Variability correlations (0.75 ENP and 0.69 WNP). These results highlight the potential of integrating deep learning and computer vision for fast and accurate TC tracking, offering a robust alternative to traditional approaches.

Keywords Tropical Cyclones Tracking · Deep Learning · Computer Vision · Atmospheric Science · Machine Learning · Multi-Object Tracking

1 Introduction

Tropical Cyclones (TCs) are among the most destructive natural phenomena (Emanuel, 2003), causing widespread damage and disruption globally. Their formation and development result from complex interactions between the ocean and atmosphere, modulated by large-scale circulation patterns. For the development of a TC, several conditions must meet (Gray, 1975; Weaver and Garner, 2023): warm sea surface temperatures from which the TC draws energy due to the evaporation, the influence of the Coriolis force along with low wind shear and ample humidity and a pre-existing low-pressure disturbance. Every year, an average of 90 TCs occur worldwide (Emanuel and Nolan, 2004), and climate change is making them stronger and more destructive (Elsner et al., 2008; Mendelsohn et al., 2012; Sun et al., 2017). Owing to their significant socio-economic impacts (World Meteorological Organization, 2023) and strong sensitivity to climate variability (Mueller et al., 2024), the accurate monitoring and prediction of TCs remains a critical challenge in both weather and climate science.

The accurate detection and tracking of these phenomena in large climate datasets is an active area of research for the climate community (Scoccimarro et al., 2014; Dabhade et al., 2021; Garner et al., 2021; Chand et al., 2022). The identification of TCs in such datasets is traditionally performed using deterministic tracking algorithms, or TC trackers (Horn et al., 2014), which detect TC structures within gridded climate fields, locate their centers, and link them across time, resulting in TC tracks (Bourdin et al., 2022). Specifically, TC tracking schemes comprise two consecutive sub-tasks: *detection* and *linking*. The detection task aims to localize TC occurrences across space and time, and is

typically highly permissive, as it detects a wide number of false positives and small disturbances. Then, the linking task joins previously detected TC occurrences across time based on some physical constraints (e.g., TC eye located in the local minima of mean sea level pressure, maximum TC distance after 6 hours etc.), further removing most of these unwanted detections.

Traditional tracking schemes are generally classified into *physics-based* (Camargo and Zebiak, 2002; Chauvin et al., 2006a; Zhao et al., 2009; Horn et al., 2014; Murakami, 2014; Zarzycki and Ullrich, 2017) and *dynamics-based* (Hodges et al., 2017a; Strachan et al., 2013; Tory et al., 2013a). Physics-based trackers rely on thermodynamic variables, typically identifying local minima in the sea level pressure and confirming the presence of a warm-core using surface temperature anomalies or geopotential thickness. They often apply an additional intensity-based criterion applied on surface wind speed or vorticity to validate detections. In contrast, dynamics-based trackers focus on vorticity fields and the velocity derivatives to detect the TC centers (Bourdin et al., 2022).

The aforementioned methods typically rely on threshold-based criteria, which makes them sensitive to expert's parameters selection and introduces potential subjectivity in their design (Dabhade et al., 2021; Enz et al., 2022). Moreover, these thresholds often vary with geographical region and TC category (Befort et al., 2020; Bloemendaal et al., 2021), leading to systematic biases and limiting the generalizability of the algorithms to regions or datasets beyond those used for calibration. In addition, TC trackers, such as those described in Hodges et al. (2017b) and Horn et al. (2014), are often computationally and data-intensive, requiring the storage and management of a considerable number of variables, at high temporal resolutions, along with extensive post-processing. As a result, the analysis of the climatic characteristics of TCs remains a resource-demanding and time-consuming task, hindering large-scale and long-term studies.

In this landscape, Machine Learning (ML) opened new avenues across key areas of climate science, including the analysis of TCs and their effect on the environment. Several studies propose innovative ML-based solutions for TC detection and tracking. A consistent part of these works frames TC identification and classification as an Object Detection (OD) task. Mask- and Faster- Region-based Convolutional Neural Networks have been employed in Wang et al. (2020); Xie et al. (2020); Nair et al. (2022), whereas the You Only Look Once architecture has been used in Shakya et al. (2020); Pang et al. (2021); Haque et al. (2022); Lam et al. (2023). Kumler-Bonfanti et al. (2020) explored U-Net-based segmentation approaches for accurate TC detection, whereas Kim et al. (2019) compared the skills of Decision Trees, Random Forest, Support Vector Machines, and Linear Discriminant Analysis for the TC classification. All the aforementioned works leverage satellite observations for training. Other studies explored TC detection with different data sources: Matsuoka et al. (2018) trained a Convolutional Neural Network (CNN) for binary classification of TCs and their precursors using Outgoing Long-wave Radiation from Cloud-resolving Global Atmospheric Simulation, whereas Galea et al. (2023) proposed TC Detect, a data-driven framework for detecting TC presence and absence leveraging ERA-Interim Dee et al. (2011) dataset for the climate variables and an online data-reduction method. Although their good performance, most of these approaches are limited to detection or classification tasks, constraining their use on climate-related applications.

Another line of research focuses its attention to the TC tracking through data-driven approaches. For example, Yan et al. (2023) defines the TROPHY framework to quantify the structural stability of TCs exploiting wind fields, making it suitable for TC tracking. Despite the innovative physics-informed approach, the algorithm doesn't computationally scale well with the number of TCs. In a more recent work, Lin et al. (2025) proposed a Bayesian Inference and Dynamic Programming Tracking (BIDTrack) method. The algorithm is optimized through a Bayesian Interval Optimization process, refining parameters to keep only statistically significant and physically consistent TC candidates, resulting in faithful TC tracks. Vaittinada Ayar et al. (2025) exploited an Ensemble Random Forest (ERF) model composed of 100 elements. The ERF is designed as a classification task, detecting TC centers and then aligning them in time with a simple tracking algorithm, achieving very good TC tracking skills.

In Accarino et al. (2023) we demonstrated the feasibility of integrating DL-based detection with a deterministic tracking scheme, using an ensemble of Deep Learning (DL) models. The TC tracker leveraged 6 input climatic drivers to train a pool of 13 DL models aimed at detecting TC centers. Subsequently, TC tracking was applied by following Zhao et al. (2009); Scoccimarro et al. (2017).

Building on the promising results of our previous work, we present *ByteStorm*, a novel framework that combines two DL models - for TC classification and localization - with BYTE (Zhang et al., 2022), a computer vision Multi-Object Tracking (MOT) algorithm for TC track reconstruction. By linking individual TC centers into coherent temporal tracks, *ByteStorm* provides an end-to-end, scalable solution for storm identification and evolution tracking. In contrast to traditional tracking schemes, *ByteStorm* relies on a data-driven framework, avoiding the need for manual thresholds tuning. Additionally, it merges the capabilities of DL models and Computer Vision algorithms for tackling TC tracking, while minimizing the number of climatic variables involved in the process. *ByteStorm*, in fact, leverages only 2 input climatic variables, considerably reducing the amount of data and computational power needed, while preserving

excellent TC tracking skills. We demonstrate the skills of ByteStorm by comparing it against four state-of-the-art deterministic tracking schemes across different metrics and analyzing its results on a couple of exemplary historical TCs.

The remainder of the paper is organized as follows: Section 2 describes the dataset generation and labeling process. Section 3 outlines the experimental setup and the evaluation metrics used to assess model performance. Section 4 presents an assessment of ByteStorm skills, while Section 5 discusses and contextualizes the findings. Finally, Section 6 draws the conclusions and outlines potential directions for future research.

2 Materials

2.1 Data Sources: IBTrACS and ERA5

2.1.1 International Best Tracks Archive for Climate Stewardship

The International Best Tracks Archive for Climate Stewardship (IBTrACS) (Knapp et al., 2010) provides the most accurate global archive of historical TCs center records. It integrates observations from 12 meteorological agencies at a 3-hourly temporal resolution and is gridded at a spatial resolution of $0.1^\circ \times 0.1^\circ$. The dataset also includes TC intensity metrics (e.g., wind speed), observation timestamps, and metadata such as the nature of the storm (e.g., Tropical, Extra Tropical, Disturbance Storm, etc.). Although IBTrACS extends back to 1841, this study focuses on the 1980-2023 period, discarding earlier records due to limited satellite coverage and excluding most recent entries that may still undergo post-processing and reanalyses, potentially compromising data reliability (IBTrACS Science Team, 2019).

2.1.2 ERA5 Reanalysis

The ERA5 reanalysis dataset (Hersbach et al., 2023) includes key climate variables that are essential for understanding TC formation. Climate variables are provided on a global regular grid at a spatial resolution of $0.25^\circ \times 0.25^\circ$, corresponding to 721×1440 (H \times W) grid points. To ensure consistency, ERA5 data are limited to the same period as IBTrACS (1980-2023). From ERA5 dataset, after some preliminary evaluation, we selected *relative vorticity at 850mb* (RV850) and *mean sea level pressure* (MSLP) among the key variables typically associated with TC events.

From a geographical perspective, in this study we focus on the Eastern and Western North Pacific (ENP and WNP, respectively) basins, two of the seven global regions where TC commonly originate (Roy and Kovordányi, 2012). This joint region is widely recognized as a particularly active one, experiencing the greatest number of cyclones each year (Roy and Kovordányi, 2012).

2.2 Dataset Processing and Augmentation

2.2.1 Data Filtering

Since 6-hourly samples of IBTrACS dataset are provided with more accurate information regarding TC characteristics than 3-hourly ones, such as the Maximum Sustained Wind (MSW) (Knapp et al., 2010), we sample both IBTrACS and ERA5 datasets at 6-hour intervals, at 00.00, 06.00, 12.00 and 18.00 UTC. Furthermore, we spatially crop the datasets over the ENP and WNP basins, covering the region $100 - 320^\circ E$ and $0 - 70^\circ N$. Although this domain partially comprises the North Atlantic (NATL) basin, we exclude that region from the evaluation phase to avoid considering partial TC tracks that start in that region and evolve above the $320^\circ E$ longitude boundary. However, it is not possible to fully exclude the area since there is a substantial number of TC events crossing both the ENP and NATL basins, that must be counted as ENP observations. This results in extracting RV850 and MSLP variables from ERA5 as gridded maps with dimensions of 280×880 grid points, corresponding to the selected spatial domain. Only tracks labeled as *main* in the "track type" field are retained from IBTrACS, while tracks marked as *provisional*, *spur*, or *provisional-spur* are discarded due to their lower reliability (IBTrACS Science Team, 2019). We consider all available storm natures in the analysis: *Not Reported* (NR), *Mixture* (MX), *Disturbance Storm* (DS), *Tropical Storm* (TS), *Extra Tropical* (ET) and *Sub Tropical* (SS). Based on the filtered IBTrACS data, we extract ERA5 maps including only time steps when a TC is recorded within the ENP or WNP basins.

2.2.2 Patches Generation and Datasets Creation

The filtering process results in a total of 36 155 maps. We divide each ERA5 map, with dimensions of 280×880 grid points and containing the two selected variables (RV850 and MSLP), into non-overlapping patches of size 40×40 , yielding 7×22 patches per map. To match spatial resolutions, we interpolate TC center coordinates from IBTrACS - originally at $0.1^\circ \times 0.1^\circ$ resolution - to match the $0.25^\circ \times 0.25^\circ$ ERA5 grid. We then assign each patch a label based

on the presence of a TC center: label 1 for patches containing a TC center (i.e., *positive patches*) and label 0 for patches that do not (i.e., *negative patches*). For each *positive patch*, since the TC center can appear anywhere within the patch, we also record the (*row*, *column*) coordinates of the TC center within the 40×40 grid (each in the range $[0, 39]$).

To train the ByteStorm DL models, we split the dataset as follows: the test set includes only TC events from the month of August between 1980-2019, chosen because it has the highest TC activity in both the ENP and WNP basins (Basconcillo et al., 2021); we then divide the remaining months from the same period into training set (1980-2009) and validation set (2010-2019). We use the August 1980-2019 subset to benchmark our model against deterministic TC trackers (see Section 4.1) and to provide robust out-of-sample performance statistics. Additionally, we use data from 2020-2023 as a second test set to evaluate the model’s ability to generalize to more recent years (see Section 4.2).

To construct the training and validation datasets, we adopt a patch-selection strategy based on the following criteria:

- **Cyclone Patches** (total: 63 300): patches that **contain** a TC center. It is important to note that the TC eye can occur at any (*row*, *column*) location of the patch, meaning the storm may be only partially visible depending on its position.
- **Nearest Patches** (total: 177 366): patches that **do not contain** a TC center but selected as the three corner-adjacent patches closest to each corresponding *cyclone patch*. This selection enriches the dataset with negative samples that may still exhibit TC-related patterns, thus improving the model’s ability to generalize. By design the number of *nearest patches* is approximately three times that of *cyclone patches*.
- **Random Patches** (total: 63 300): additional **non-cyclone** patches randomly sampled from the remaining 7×22 grid, excluding those already designated as **nearest patches**. One random patch is selected per *cyclone patch*, ensuring numerical balance.

This sampling strategy results in a *positive-to-negative* patch ratio of approximately 1:4. To address this class imbalance, we apply data augmentation to *positive patches* using affine transformations: (i) 180° rotation, (ii) horizontal flip, and (iii) vertical flip. These augmentations help in balancing the dataset and enhance model’s generalization capabilities by exposing it to a broader range of data configurations.

3 Methods

3.1 Experimental Setup

The experimental setup of ByteStorm consists of two main steps:

1. Two DL models, (i.e., *classification*, *localization*) are jointly used to detect TC center locations;
2. The BYTE MOT algorithm (Zhang et al., 2022) is used to align TC center detections over time, thus reconstructing full TC tracks.

In particular, the *classification* model assigns a probability of TC occurrence to each patch, and, if a patch is classified as containing a TC phenomena (probability ≥ 0.5 , where 0.5 represents the canonical logistic threshold), the *localization* model estimates the TC center coordinates within that patch. Figure 1 shows a high-level overview of the ByteStorm TC tracking algorithm. It first partitions the input drivers into non-overlapping patches (see Section 2.2.2) and feeds them into the *classification* model. If the classifier determines the presence of TCs within the patches, the *localization* model is used to determine their location. By applying the two DL models on a set of consecutive 6-hourly maps, a wide number of TC locations is detected. Finally, ByteStorm employs the BYTE algorithm to link the TC centers into spatio-temporal tracks. The following subsections present the different steps of the algorithm.

3.1.1 TC Detection: Classification and Localization DL models

In this work, we split the TC Detection task into two sub-tasks, namely *classification* and *localization*. We jointly train two separate DL models, both leveraging the same Visual Geometry Group (VGG) model (Simonyan and Zisserman, 2015). We treat the two physical drivers (i.e., RV850 and MSLP) within each patch as 2-dimensional images stacked together, yielding an input of size $2 \times 40 \times 40$. The VGG networks then process the drivers, specifically:

- **Classification Model** - learns the relationship associated with a potential TC phenomena from the input drivers and estimates the probability of TC occurrence through a sigmoid activation function in the output layer. It is trained on the Training Dataset described in section 2.2.2, including *nearest*, *random* and the data-augmented *cyclone patches*. The loss function used is the Binary Cross Entropy (BCE):

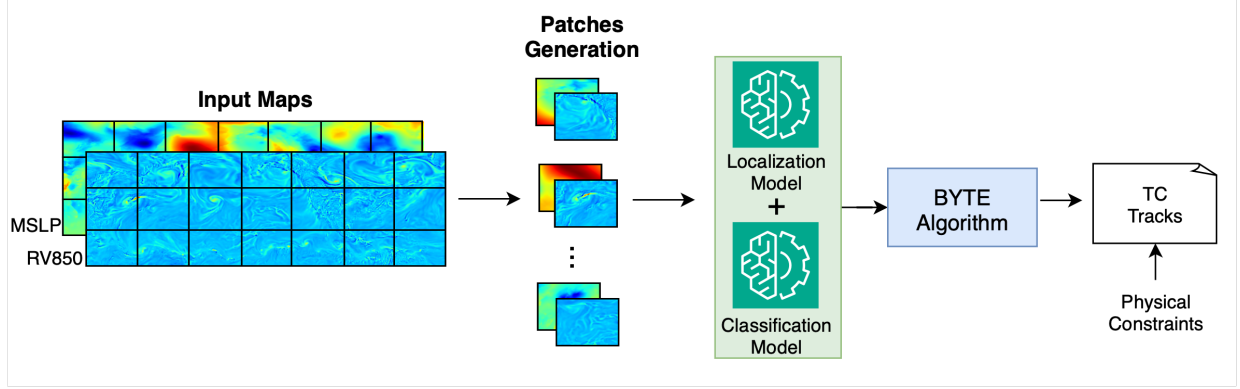


Figure 1: Overview of the ByteStorm approach. The input maps, consisting of RV850 and MSLP drivers, are divided into non-overlapping patches and processed by two models to (i) detect the TCs and (ii) locate their position within the patch. The BYTE method is then applied to link TC center detections into coherent spatio-temporal tracks.

$$\mathcal{L}_{BCE} = -\frac{1}{N_1} \sum_{i=1}^{N_1} y_i \log p_i + (1 - y_i) \log(1 - p_i) \quad (1)$$

where N_1 is the number of patches in the dataset (i.e., *cyclone + nearest + random patches* for the classification task), y_i is the ground truth label (0 or 1) of the i -th dataset sample, while p_i is the probability score of i -th dataset sample estimated by the DL model.

- **Localization Model** - learns to recognize the TC related patterns and to estimate the local TC center coordinates expressed as (row, col) within the 40×40 patch. It is trained exclusively on the data-augmented *cyclone patches* using the Mean Absolute Error (MAE) as loss function:

$$\mathcal{L}_{MAE} = \frac{1}{N_2} \sum_{i=1}^{N_2} |y_i - \hat{y}_i| \quad (2)$$

where N_2 is the number of dataset's elements (i.e., *cyclone patches* for the localization task), y_i are the true (row, col) coordinates and \hat{y}_i is the predicted TC center coordinates.

As shown in Figure 2, the two VGG networks start with a backbone composed of 6 CNN (Lecun et al., 1998) Blocks followed by 4 Linear Blocks and the output head. Each of the CNN Blocks comprises 3 convolutional layers with 3×3 kernel size, interleaved with ReLU activation function and ending with a Max Pooling layer to halve the spatial image size. The number of filters doubles at each block, from 32 to 1024. The CNN Blocks ensure to capture complex spatial non-linear patterns related to TC occurrence, processing the multi-scale interaction between the two physical drivers directly in the latent space. The Linear Blocks, instead are composed of Linear layers interleaved with ReLU activation function. These blocks learn to translate the spatial information coming from the CNN into an encoded vector containing the information related to the TC position in the case of *localization* model, or the TC presence in the case of *classification* model. The number of filters in this case is 1024, 512, 512, 256. After the CNN and Linear blocks, we apply a model-specific output layer. *Classification* model has a scalar value in output after a sigmoid activation function that constrains the values between 0 and 1. *Localization* model has two values in output, to predict a (row, col) coordinate. Additionally, whereas the *Classification* model is initialized with default weights, the *Localization* one is initialized with Normal distribution with 0 mean and 0.03 standard deviation. This operation increased the magnitude of the weights, enabling the *Localization* model to output values in the range $[0, 39]$. We perform training with AdamW optimization (Loshchilov and Hutter, 2019), with a batch size of 8192 for 150 epochs.

Based on our experiments, considering the relatively small dataset, this 11M parameters' network configuration is balanced enough to ensure a good trade-off between bias and variance, thus avoiding both over- and under-fitting problems.

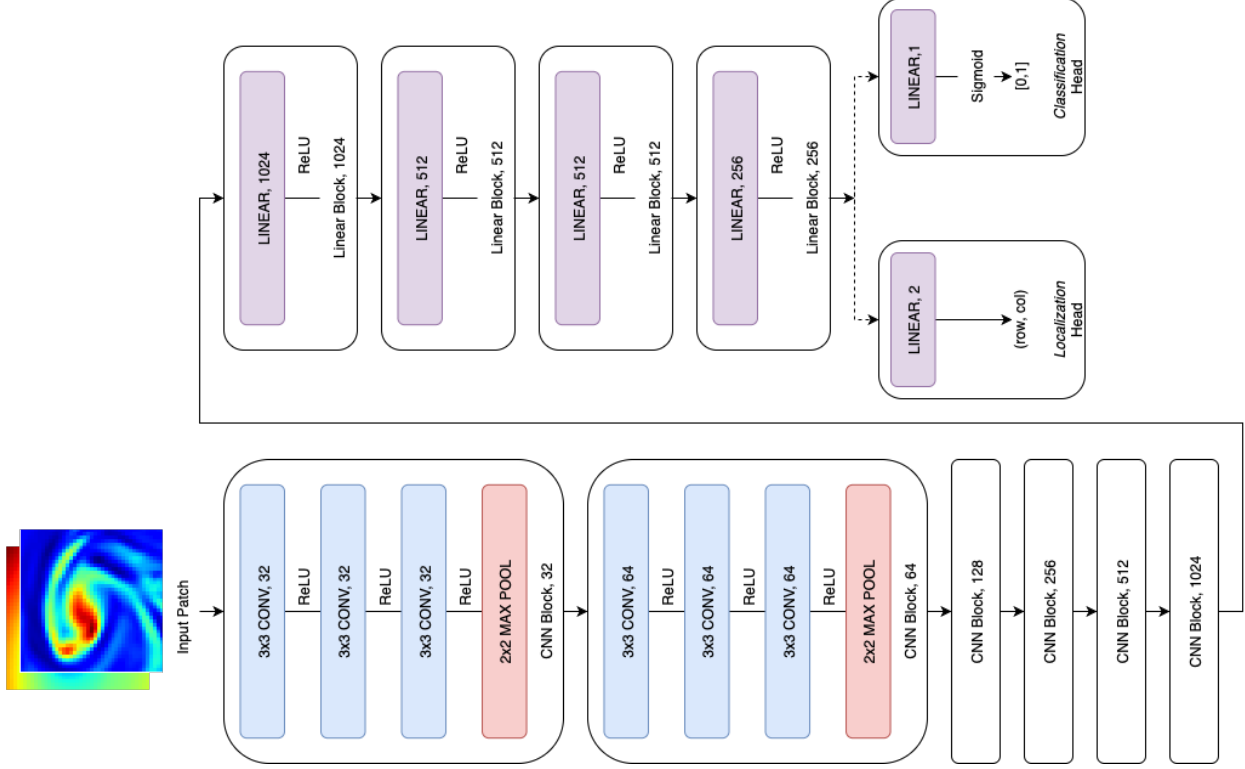


Figure 2: Architecture of the VGG-like models used in this work. A series of 6 CNN blocks is used as convolutional backbone. The CNN model is followed by a series of 4 Linear blocks that decode the spatial information coming from the CNN into a representation of TC presence/absence in the case of *Classification* model or the location of the TC eye in the case of *Localization* model. $f(x)$ is the ReLU activation function.

3.1.2 Tracking Algorithm: BYTE

BYTE is an algorithm widely used in the Computer Vision domain for MOT (Zhang et al., 2022). BYTE is a simple yet effective data-association method. In contrast to other data-association algorithm, BYTE retains almost every detection box, separating them in low- and high-score ones.

The algorithm can be tuned through several hyper-parameters: the *Track Buffer* defines the maximum number of frames (i.e., 6-hourly time-steps in our case) that can miss after which a track is labeled as *lost*; *Track Threshold* sets the confidence upper bound to consider a detection as valid; and the *Match Threshold* defines the minimum Intersection-over-Union (IoU) overlap required to join two consecutive detections to the same track.

In this work, TC centers predicted by the *localization* model are labeled with the probability score estimated by the *classification* model and enclosed in a bounding box of size 21×21 pixels. The boxed detections are then processed by BYTE to reconstruct the TC tracks. To ensure physical consistency, BYTE’s outputs are post-processed with additional physical constraints. We discard detections originated above 30° of latitude, similarly to other state-of-the-art TC trackers (Hodges et al., 2017b). Furthermore, following Scoccimarro et al. (2017) and Zhao et al. (2009), we tune the bounding box size and other hyper-parameters to enforce maximum TC displacements of 400 km between consecutive 6-hourly time-steps, and discard all the tracks lasting less than 3 days (i.e., equivalent to 12 6-hourly time-steps). Appendix A.1 provides full details on BYTE’s parameters tuning.

3.2 Evaluation Metrics

To assess the generalization capabilities of ByteStorm, we evaluate its performance on out-of-sample data and against some state-of-the-art deterministic tracking schemes, such as OWZ (Tory et al., 2013b), UZ (Ullrich et al., 2021), CNRM (Chauvin et al., 2006b) and TRACK (Hodges et al., 2017b), following the approach in Bourdin et al. (2022). We adopt Several evaluation metrics, including *Probability Of Detection* (POD), *False Alarm Rate* (FAR), *Track Duration*, *Inter-Annual Variability* (IAV) and *Track Smoothness*.

POD and FAR: are commonly used to evaluate the skills of TC trackers. These are computed as follows:

$$POD = \frac{H}{H + M} \quad (3)$$

$$FAR = \frac{FA}{H + FA} \quad (4)$$

Where Hit (H) is the number of observed TC tracks that are correctly matched to at least one detected TC track during the TC lifetime, Miss (M) is the number of observed track with no corresponding detected TC track, while False Alarms (FA) is the number of detected TC tracks that do not correspond to any observed one.

Interannual Variability (IAV): describes the year-to-year fluctuations in TC frequency. In this study, we compute it only for the month of August over the 40 years period, as this month was selected for the test set. IAV represents the number of TC tracks detected in this target month of each year, allowing a comparison of the temporal series reconstructed by the trackers. To assess whether the TC trackers correctly follow the real IAV, we compute the Pearson correlation coefficient between each tracker and the IBTrACS historical records. Before computing the correlation, we de-trend the IAV to align the IAV records and avoid fluctuations in correlation values.

Track Duration: measures the distribution of TC track lengths (in days) and serves to assess whether trackers correctly capture the temporal extent of cyclones. It highlights potential biases in underestimating or overestimating the duration of TC events.

Track Smoothness: measures how much the direction of a TC varies during its lifetime, giving information about the shape of the track. We compute it as the standard deviation of the bearing angle variation (see below) between each consecutive detection. The lower the standard deviation is, the lower the TC centers change direction over time. Instead, if the smoothness value is high, it likely means that the detected TC track is noisier. Ideally, the predicted TC track should be as smooth as the variation shown in the IBTrACS ground truth.

Given a set of latitude and longitude coordinates (ϕ_i, λ_i) for $i = 1, \dots, N$, the bearing between points can be computed as in Bearing Angle Computation (Veness, 2022).

$$\theta_i = \tan^{-1}(\sin(\Delta\lambda_i) \cos(\phi_{i+1}), \cos(\phi_i) \sin(\phi_{i+1}) - \sin(\phi_i) \cos(\phi_{i+1}) \cos(\Delta\lambda_i)) \quad (5)$$

where $\Delta\lambda_i = \lambda_{i+1} - \lambda_i$. Then the variation between successive bearings is:

$$\Delta\theta_i = \min(|\theta_{i+1} - \theta_i|, 2\pi - |\theta_{i+1} - \theta_i|) \quad (6)$$

Hence, the Track Smoothness score is defined as the standard deviation σ of the angular variations:

$$\sigma_{smoothness} = \sqrt{\frac{1}{N-2} \sum_{i=1}^{N-2} (\Delta\theta_i - \bar{\Delta}\theta)^2} \quad (7)$$

To compute the aforementioned metrics, we define a matching algorithm between IBTrACS ground truth and the TC Tracker's tracks. For each time-step t_i , each detected TC center d_i is matched with all the observed (IBTrACS) TC centers o_i that are closer than 300 km with respect to d_i . We refer to Bourdin et al. (2022) for a deeper explanation of the matching procedure.

4 Results

4.1 Comparison against Deterministic TC trackers

In the following subsections, we compare ByteStorm with four well-known deterministic trackers through a per-basin evaluation, highlighting the key strengths of the DL-based method. Taking inspiration from Bourdin et al. (2022), we select for the evaluation the trackers CNRM and UZ (physics-based trackers), and OWZ and TRACK (dynamic-based trackers). These trackers differ in terms of variables, thresholds and methodologies considered for TC detection and tracks reconstruction. The four trackers can thus lead to very different results in terms of TC tracks effectively detected and false alarms, providing a proper comparison framework for ByteStorm.

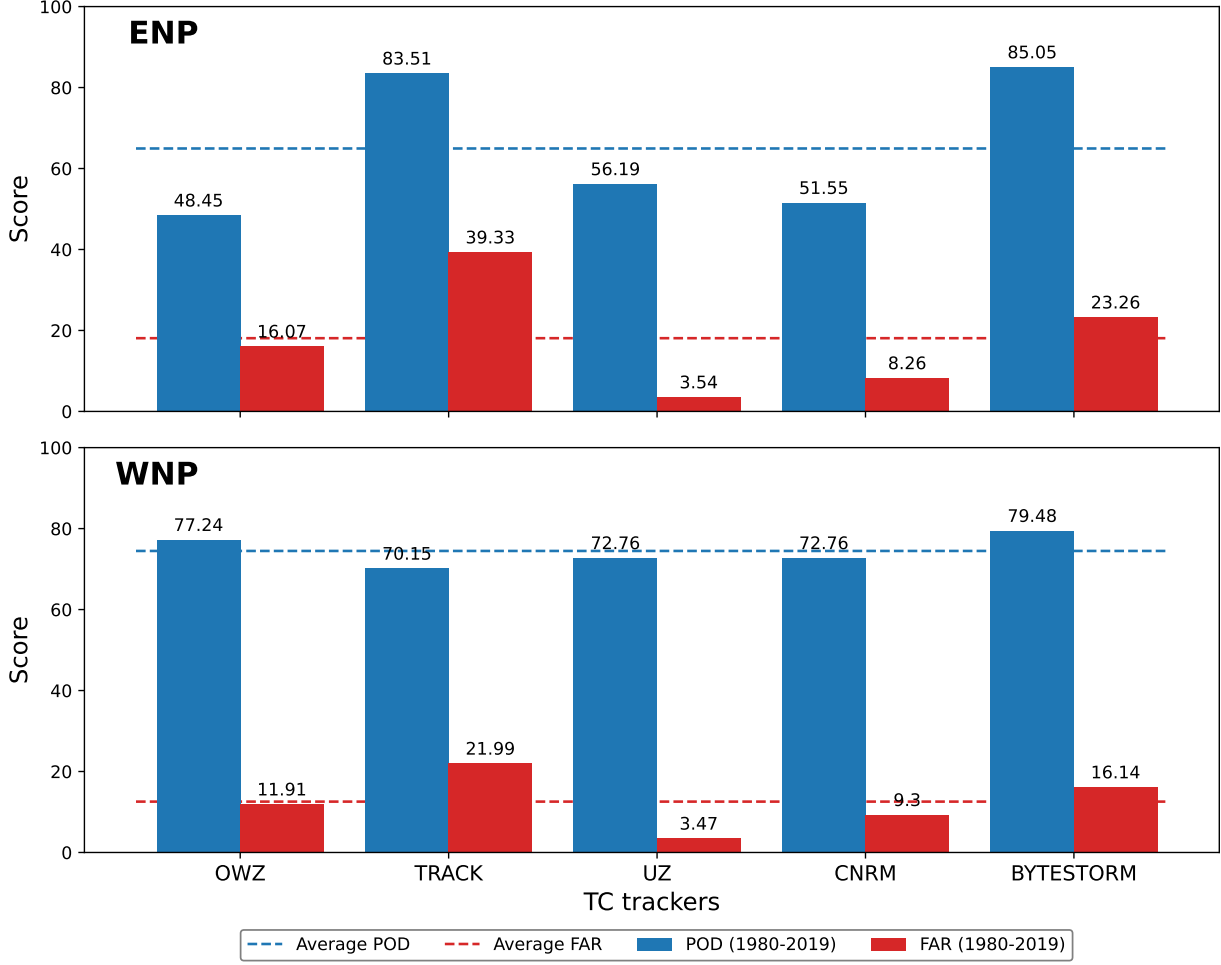


Figure 3: Probability of Detection (POD) - higher is better - and False Alarm Rate (FAR) - lower is better - of the deterministic TC trackers compared with ByteStorm, on the ENP (top) and WNP (bottom) basins.

We evaluate ByteStorm tracking skills against the filtered IBTrACS dataset described in 2.2.1. To ensure a more comprehensive skill assessment, the ground truth also includes not well formed TC tracks, i.e., TC records labeled as NR, MX and DS (see subsection 2.2.1) in the IBTrACS documentation (IBTrACS Science Team, 2019).

4.1.1 Probability Of Detection and False Alarm Rate

POD and FAR on the ENP basin in Figure 3 (top panel) clearly shows that ByteStorm outperforms three of deterministic trackers (i.e., OWZ, UZ and CNRM) in terms of POD by $\sim 30\%$ while being slightly better than TRACK by $\sim 1.5\%$. The FAR metric, instead, is 23.26%, meaning that it is higher than the other trackers but better than TRACK algorithm (39.33%).

Regarding the WNP basin (Figure 3, bottom panel), POD values are overall more balanced among the TC trackers, with ByteStorm yielding the highest value (79.48%). Furthermore, in the same region, it shows a lower FAR (16.14%), yet still higher than OWZ (11.91%), UZ (3.47%) and CNRM (9.3%), but visibly lower than TRACK (21.99%).

These two metrics reflect a trade-off between correctly reconstructed TC tracks and false positives. Contrary to deterministic trackers, ByteStorm shows more balanced skills in terms of POD and FAR in both the considered basins.

4.1.2 Inter-annual Variability

The IAV of the different trackers is shown in Figure 4. ByteStorm (red line) closely follows the observed IBTrACS variability (blue line) on both the ENP and WNP basins. We compute the Pearson correlation coefficient (denoted with

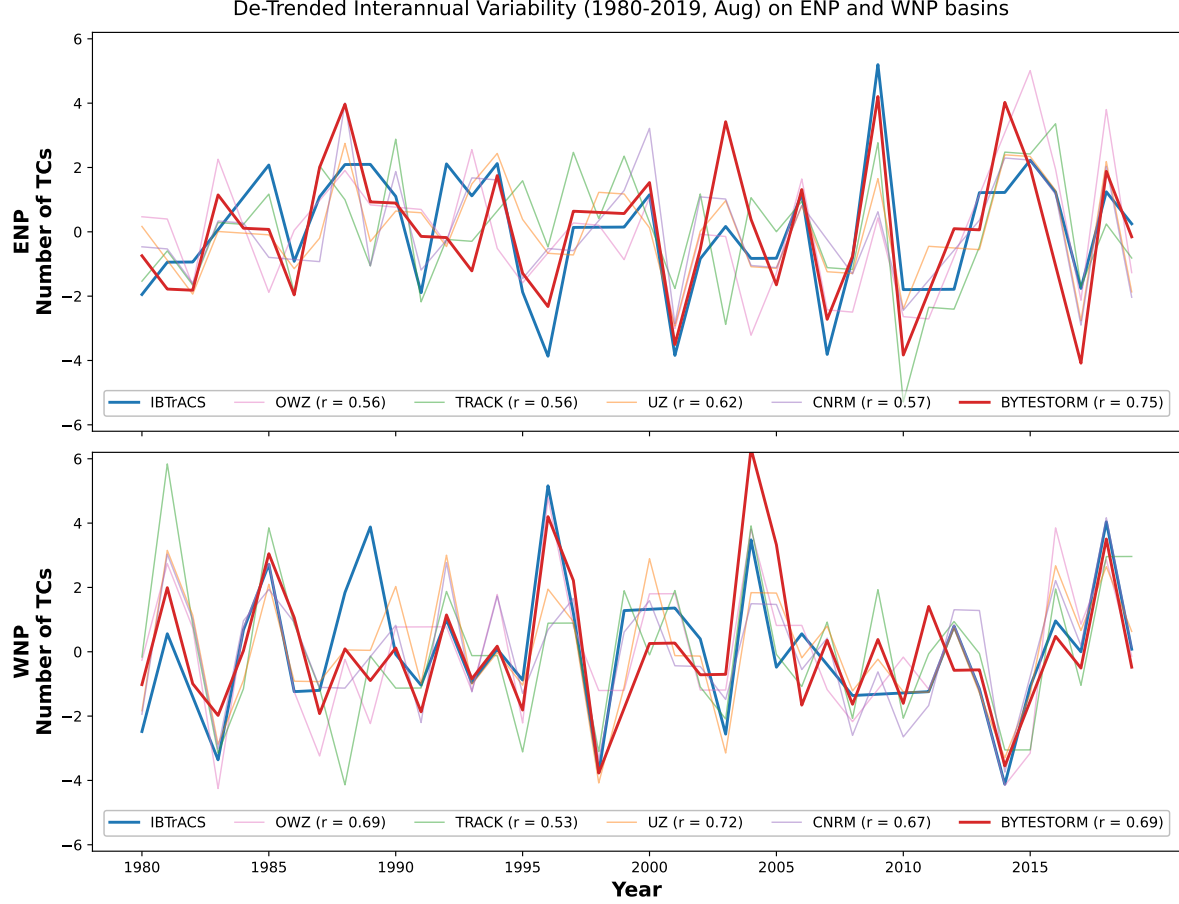


Figure 4: De-Trended Inter-Annual Variability (IAV) of deterministic TC trackers compared to ByteStorm on ENP (top) and WNP (bottom) basins. ByteStorm is shown with a red thicker line.

r in the Figure’s labels) between IAV of IBTrACS observations and the IAV of the TC trackers on the August month across 40 years of data (see Section 3.2). Despite having high correlations, most of deterministic TC trackers perform worse than our approach. In fact, on the ENP basin ByteStorm outperforms all the other trackers with a correlation value $r_{ENP} = 0.75$. Over the WNP basin, it achieves a correlation value $r_{WNP} = 0.69$, comparable to most deterministic trackers, with the exception of UZ ($r_{WNP} = 0.72$).

As stated in Section 2.2.2, August is the most active month across the basins considered in this study. ByteStorm’s ability to capture IAV with high correlation on the test set reflects its strong generalization skills on out-of-sample data.

4.1.3 Track Duration

Figure 5 shows the track duration of each tracker with respect to IBTrACS historical observations. Each tracker closely follows the ground truth (reported in blue). UZ (orange) and CNRM (violet) underestimate the real TC duration on the test set, while TRACK overestimates both the number of TC days and the overall track duration, as well. Although ByteStorm closely follows the real TC duration, there is a large number of short tracks (i.e., TC tracks that last less than 3-4 days) which mostly correspond to false alarms.

4.1.4 Track Smoothness

In Figure 6, we report the Track Smoothness of IBTrACS and the TC trackers. For each different TC track within the considered subset (IBTrACS or a TC Tracker), we compute the smoothness as in Section 3.2. We report the resulting set of smoothness scores in the box-plots in Figure 6. Each box-plot contains the track smoothness values between the 1st and 3rd quartiles, whereas the horizontal bar within each box is the median value of the distribution. ByteStorm

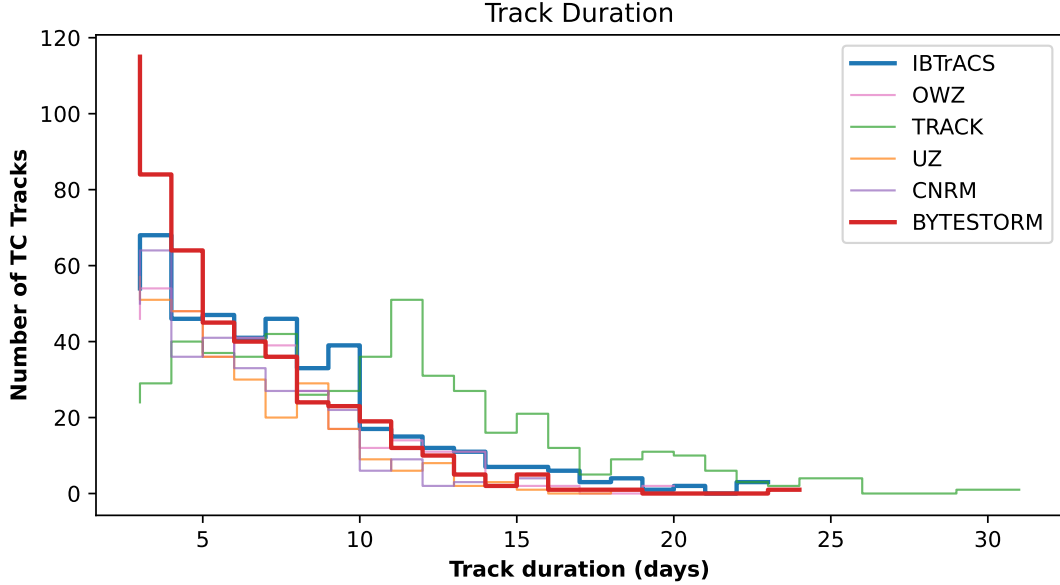


Figure 5: Track Duration is represented as the number of TCs (y-axis) lasting for a certain amount of days (x-axis). All the tracking schemes closely follow IBTrACS historical observations.

is the only TC tracker that provides considerably smooth TC tracks, much lower than the other trackers from the state-of-the-art, and hence closer to the IBTrACS ground truth. It is worth noting that ByteStorm’s median value (18.77) is slightly higher than the IBTrACS 3rd quartile (16.04), enforcing the meaningfulness of ByteStorm smoother tracks with respect to the other TC trackers.

This result demonstrates that the complementary use of DL models and BYTE algorithm is able to provide smooth TC tracks with good consistency between consecutive time-steps, although the DL models are not trained to explicitly account for the temporal dimension.

4.1.5 Test Cases: Results on the 5 longest tracks

To better assess the skills of ByteStorm, we conduct a comparison with respect to the 5 longest TC tracks. Among the TC tracks available within the Test Set, we select the 5 longest TCs, namely: Abby (1983), Keoni (1993), John (1994), Guillermo (1997) and Dora (1999). In this section, for the analysis we present only TC Abby and TC John, while we report the other TCs in Appendix A.2, jointly with general information about the selected TCs.

Figure 7 shows the observed tracks of TCs Abby (left panel) and John (right panel) from IBTrACS (in blue), alongside the corresponding detections by ByteStorm (in red). We overlay both observed and detected TC tracks on a map of MSLP minimum from ERA5, obtained computing the minimum over each time-step of the TC track. This visualization highlights the low-pressure centers associated with each TC, aiding their spatial localization.

Tropical Cyclone Abby

Regarding TC Abby, it is important to note that during the early stages of formation, highlighted in the zoomed section of the left panel, ERA5 data shows a displaced MSLP minimum, located to the right of the historical track reported by IBTrACS. As a result, all the TC trackers, including ByteStorm, align with the ERA5 data and produce similar shifted TC centers, as shown in Figure A.2. This discrepancy stems from a well-known limitation of ERA5 and other reanalysis products, which often poorly assimilate TCs (Slocum et al., 2022; Bian et al., 2021), leading to inconsistencies in storm intensity and position relative to IBTrACS observation. Additionally, according to IBTrACS Science Team (2019), IBTrACS provides TC centers with an uncertainty in the position which is inversely proportional to the storm intensity.

Despite the mismatch between ERA5 and IBTrACS in the positioning of TC centers, ByteStorm maintains physical consistency with ERA5 data by following the low-pressure basin in line with the other trackers (see Figure A.2 and Section A.2.2).

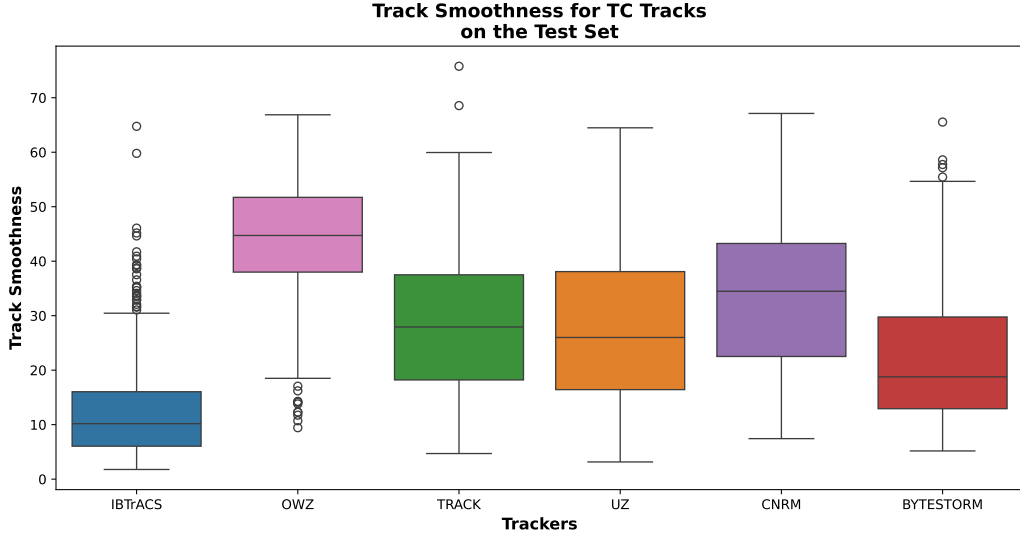


Figure 6: Track Smoothness box-plots of IBTrACS (blue box, left) compared with deterministic models (pink, green, orange and purple) and ByteStorm (red, right). For each TC track, the Track Smoothness is computed as the standard deviation of the variation of the bearing angle between each consecutive detection within the track. The resulting sets of Track Smoothness scores was used to compute meaningful statistics in the form of box-plots.

As TC Abby intensifies, ByteStorm’s detections become more closely aligned with the observations, demonstrating its ability to extrapolate TC position from the local MSLP minima. After landfall in central Japan, ByteStorm’s detections shift northward, likely influenced by the underlying land-sea contrast introduced by the presence of Japanese islands.

Tropical Cyclone John

TC John was considered for long time one of the most intense cyclonic phenomena ever recorded in the Pacific. In right panel of Figure 7, we report TC John when its strength started increasing, gaining energy. The image clearly shows the low-pressure minima, with dark spots centered over the historical TC records (in blue). ByteStorm easily captures the TC centers with good accuracy, as demonstrated by the zoomed section of the figure. As the storm starts weakening (left side of the panel), the ByteStorm detects the TC centers with lower accuracy.

4.2 Extrapolation on recent years

To assess the robustness of the proposed approach on a recent temporal scale, we perform an evaluation over values out of the training range, the period 2020-2023. We avoid the direct comparison with deterministic TC trackers in this phase as Section 4.1 already provides a comprehensive and statistically significant evaluation of ByteStorm skills. Additionally, this evaluation aims at understanding the capabilities in temporal extrapolation of the proposed approach.

Regarding POD and FAR, ByteStorm obtains very good skills in detecting TCs under never seen conditions, also representing the real seasonal behavior from IBTrACS (Figure 8). On the ENP basin, POD and FAR are 89.71% and 21.79%, respectively. On the WNP basin, instead, the POD = 86.17% and FAR = 22.12%.

Seasonal TC distribution in Figure 8 reports the distribution of TC genesis (y-axis) over the test set on a monthly scale (x-axis). It is clear from the figure that ByteStorm correctly represents the seasonality of TC occurrence, meaning that it is able to capture the most meaningful seasonal behavior directly from the data.

5 Discussion

ByteStorm demonstrates clear advantages over traditional deterministic trackers, achieving higher accuracy and improved representation of TC inter-annual variability while demanding low computational resources.

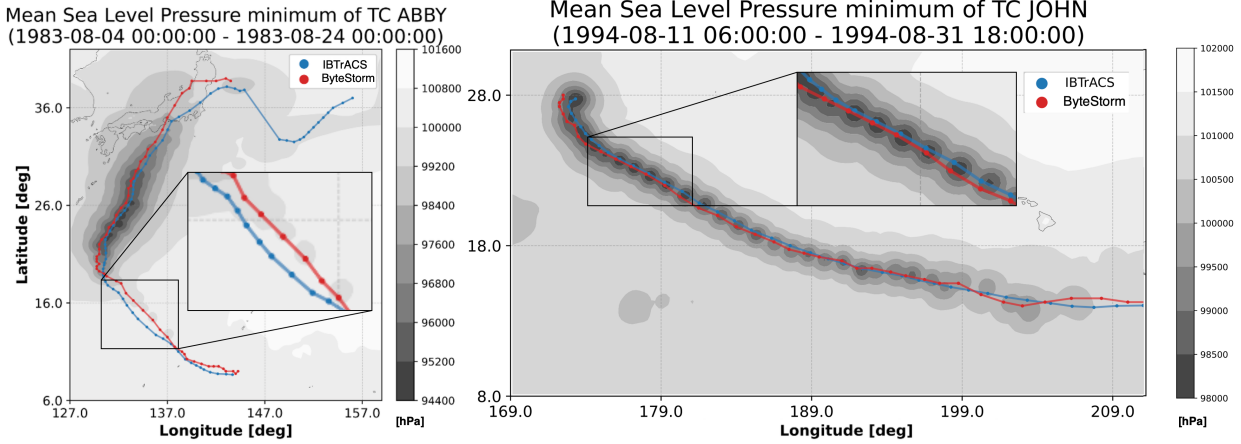


Figure 7: Abby (left panel) and John (right panel) TC tracks are reported in the figure. IBTrACS historical TC occurrences are reported in blue, while TC tracks produced by ByteStorm are reported in red. The resulting TC tracks are overlaid onto the Mean Sea Level Pressure minimum computed over the entire historical TC track, in order to enhance the low-pressure minima associated with the TC during its lifetime.

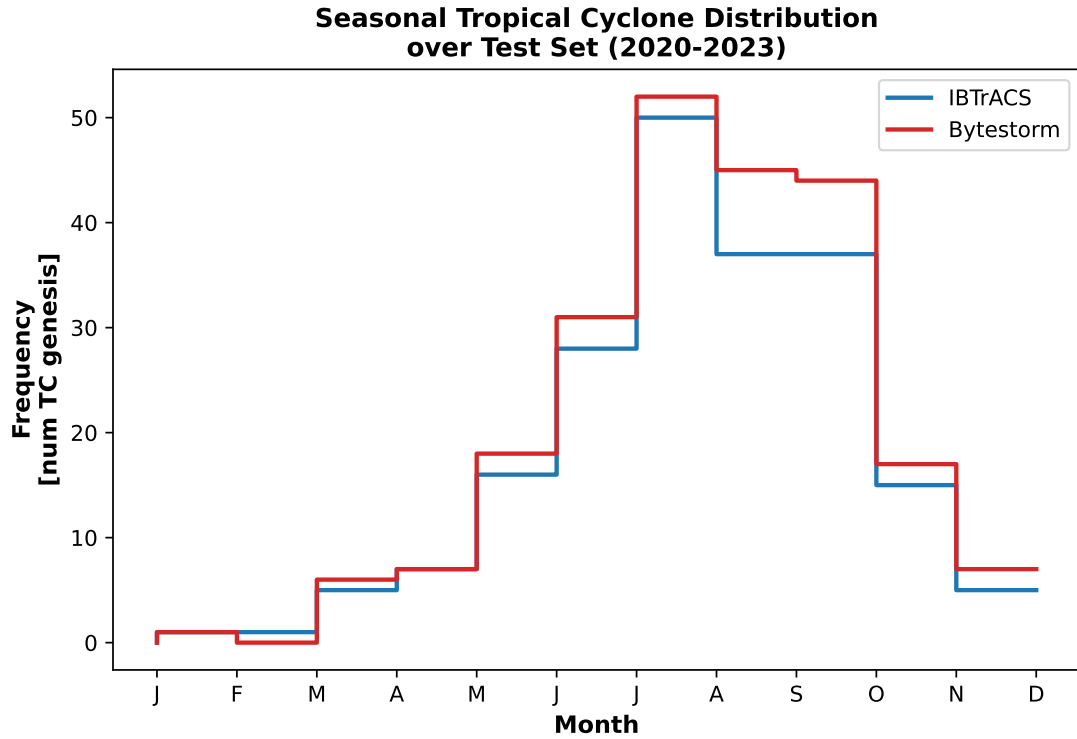


Figure 8: Seasonal Tropical Cyclones distribution over the 2020-2023 period. The number of TC genesis is reported on the y-axis and the month on the x-axis. Our TC tracker frequency is reported in red, and the IBTrACS ground truth in blue.

The experiments are carried out leveraging the Juno hybrid cluster, one of the High Performance Computing (HPC) systems available at the CMCC HPC Center. The two models are trained on 4 GPUs NVidia Volta A100 with 40GB of RAM, while the evaluation on the test set is executed on a single GPU.

A key strength of the approach lies in its simplicity, as the two models operate using only two physical drivers, i.e., RV850 and MSLP. Despite the limited number of variables, the two-stage architecture is capable of learning the physical patterns related to TC occurrence and locating its geographical position. Then, the physically constrained data-association method used for the TC tracking, i.e. BYTE, enables reliable and smooth TC tracks, comparable or even better than the deterministic tracking approaches.

ByteStorm is either equal or superior in terms of skills to existing deterministic methods and achieves the highest POD in both ENP and WNP basins, while obtaining competitive FAR (as depicted in Figure 3). Importantly, it also shows stable and consistent results across basins, showing good detection skills and reduced dependency in basin-specific tuning. The ability of the model to maintain this balance is critical in TC tracking, as often conventional approaches report different skills across basins (Bourdin et al., 2022).

Beyond classical metrics, ByteStorm excels in capturing IAV. It exhibits one of the strongest correlations with IBTrACS historical data (see Figure 4), indicating that our TC tracker captures the historical frequency of TCs on never seen data. ByteStorm also demonstrates competitive performance in track duration estimation, which closely matches the distribution of historical cyclone lifetimes. Although an over-representation of short tracks is observed, mainly due to false positives, the model still reproduces the overall duration profile with high fidelity (see Figure 5). In addition, track smoothness provides further evidence of the tracker robustness by quantifying the coherency of the reconstructed tracks. In contrast to some deterministic approaches that exhibit noisy TC detections along the track or over-extended tracks, ByteStorm is able to maintain smooth TC tracks throughout the cyclone lifetime (Figure 6).

Finally, a case study on the five longest TC tracks confirms the ByteStorm’s robustness, which captures most of the cyclone path during intense phases and produces realistic and smooth tracks (as shown in Figure 7). As stated in Section 4.1.5, our TC tracker is consistent with the TC-related patterns in the ERA5 dataset.

Among the limitations of ByteStorm, the models still lack the capability to forecast the TC intensity along with its position, an aspect that is relevant in the literature. Moreover, ByteStorm outputs many short tracks (i.e., lasting less than 4 days), that are mostly linked to False Alarms. Further analysis is required to mitigate the limitation. Finally, using two different CNNs, for classification and localization, requires the training of both the models, increasing the training time. Carefully merging the two DL architectures could mitigate this limitation.

6 Conclusions

In this work, we present a cutting-edge DL-based framework for TC tracking that combines a two-stage TC Detection model with the BYTE algorithm. ByteStorm demonstrates superior performance, in most cases, compared to traditional deterministic trackers across several evaluation metrics. Moreover, contrary to traditional methods which are extremely demanding in terms of computational resources, ByteStorm enables fast and reliable TC diagnostics. Consequently, the study of TC characteristics can be carried out much more quickly, flexibly, and cheaply, thereby significantly broadening both the potential user base and the range of possible studies that can be conducted.

The specific design allows independent optimization of Classification and Localization, enabling the possibility to focus and improve each task separately. Moreover, the method exhibits strong generalization capabilities across the considered TC formation basins, highlighting its robustness and potential applicability over different basins with minimal re-training or fine-tuning effort. Additionally, the computational efficiency and scalability of the framework further support its suitability for operational monitoring and real time TC tracking and monitoring.

Looking ahead, different promising directions emerge to enhance the current framework. Exploring other of DL techniques or embedding physical constraints within the data-driven approach, may enable better performance in the detection/localization task, thus enhancing the overall tracker robustness. Furthermore an important direction is the development of a unified model capable of jointly performing all tasks together while also predicting additional key TC-related information such as intensity and direction.

Finally, future work will prioritize validating the framework across different basins and its integration in Earth System Models as a diagnostic tool, enabling real-time TC diagnostics as a direct output of climate simulations. This will pave the way for more effective and reliable monitoring and forecasting of TCs on a global scale.

CRediT authorship contribution statement

Davide Donno: Writing – original draft, Visualization, Methodology, Investigation, Software, Data curation, Validation

Donatello Elia: Writing – original draft, Visualization, Methodology, Conceptualization, Investigation, Supervision, Validation

Gabriele Accarino: Writing - Review & Editing, Methodology, Conceptualization, Data Curation, Validation

Marco De Carlo: Writing – original draft, Visualization, Investigation, Software, Validation

Enrico Scoccimarro: Writing - Review & Editing, Conceptualization, Visualization, Validation

Silvio Gualdi: Writing - Review & Editing, Conceptualization, Visualization, Validation

Funding

This work was supported in part by the interTwin project. interTwin has received funding from Horizon Europe under grant agreement No 101058386.

Computer Code Availability

- Software name: *ByteStorm*
- Programming language: Python
- Software requirements: UNIX, PyTorch, Xarray, Numpy, Pandas
- Hardware requirements: It is recommended to use a system equipped with one or more GPUs and at least 32 GB of RAM.
- Source code is available for downloading at: <https://github.com/CMCC-Foundation/bytestorm>
- Program size: 131 MB considering the provided repository. The whole dataset that we used is 200 GB.

Data availability

Datasets used for model development and training

- ERA5 single levels dataset: <https://cds.climate.copernicus.eu/datasets/reanalysis-era5-single-levels?tab=overview>
- ERA5 pressure levels dataset: <https://cds.climate.copernicus.eu/datasets/reanalysis-era5-pressure-levels?tab=overview>
- IBTrACS dataset: <https://www.ncei.noaa.gov/products/international-best-track-archive>

References

Accarino, G., Donno, D., Immorlano, F., Elia, D., Aloisio, G., 2023. An ensemble machine learning approach for tropical cyclone localization and tracking from era5 reanalysis data. *Earth and Space Science* 10, e2023EA003106. URL: <https://agupubs.onlinelibrary.wiley.com/doi/abs/10.1029/2023EA003106>, doi:doi:<https://doi.org/10.1029/2023EA003106>, arXiv:<https://agupubs.onlinelibrary.wiley.com/doi/pdf/10.1029/2023EA003106>. e2023EA003106 2023EA003106.

Basconcillo, J., Cha, E.J., Moon, I.J., 2021. Characterizing the highest tropical cyclone frequency in the Western North Pacific since 1984. *Scientific Reports* 11, 14350. URL: <https://www.nature.com/articles/s41598-021-93824-2>, doi:doi:10.1038/s41598-021-93824-2.

Befort, D.J., Kruschke, T., Leckebusch, G.C., 2020. Objective identification of potentially damaging tropical cyclones over the western north pacific. *Environmental Research Communications* 2, 031005. URL: <https://dx.doi.org/10.1088/2515-7620/ab7b35>, doi:doi:10.1088/2515-7620/ab7b35.

Bian, G.F., Nie, G.Z., Qiu, X., 2021. How well is outer tropical cyclone size represented in the ERA5 reanalysis dataset? *Atmospheric Research* 249, 105339. URL: <https://linkinghub.elsevier.com/retrieve/pii/S016980952031276X>, doi:doi:10.1016/j.atmosres.2020.105339.

Bloemendaal, N., de Moel, H., Mol, J.M., Bosma, P.R.M., Polen, A.N., Collins, J.M., 2021. Adequately reflecting the severity of tropical cyclones using the new tropical cyclone severity scale. *Environmental Research Letters* 16, 014048. URL: <https://dx.doi.org/10.1088/1748-9326/abd131>, doi:doi:10.1088/1748-9326/abd131.

Bourdin, S., Fromang, S., Dulac, W., Cattiaux, J., Chauvin, F., 2022. Intercomparison of four algorithms for detecting tropical cyclones using ERA5. *Geoscientific Model Development* 15, 6759–6786. URL: <https://gmd.copernicus.org/articles/15/6759/2022/>, doi:doi:10.5194/gmd-15-6759-2022.

Camargo, S.J., Zebiak, S.E., 2002. Improving the detection and tracking of tropical cyclones in atmospheric general circulation models. *Weather and Forecasting* 17, 1152 – 1162. URL: https://journals.ametsoc.org/view/journals/wefo/17/6/1520-0434_2002_017_1152_itdato_2_0_co_2.xml, doi:doi:[https://doi.org/10.1175/1520-0434\(2002\)017<1152:ITDATO>2.0.CO;2](https://doi.org/10.1175/1520-0434(2002)017<1152:ITDATO>2.0.CO;2).

Chan, J.C.L., 1986. Supertyphoon abby—an example of present track forecast inadequacies. *Weather and Forecasting* 1, 113 – 126. URL: https://journals.ametsoc.org/view/journals/wefo/1/3/1520-0434_1986_001_0113_saeopt_2_0_co_2.xml, doi:doi:10.1175/1520-0434(1986)001<0113:SAEOPT>2.0.CO;2.

Chand, S.S., Walsh, K.J., Camargo, S.J., Kossin, J.P., Tory, K.J., Wehner, M.F., Chan, J.C., Klotzbach, P.J., Dowdy, A.J., Bell, S.S., et al., 2022. Declining tropical cyclone frequency under global warming. *Nature Climate Change* 12, 655–661. doi:doi:10.1038/s41558-022-01388-4.

Chauvin, F., Royer, J.F., Déqué, M., 2006a. Response of hurricane-type vortices to global warming as simulated by ARPEGE-climat at high resolution. *Climate Dynamics* 27, 377–399. URL: <https://doi.org/10.1007/s00382-006-0135-7>, doi:doi:10.1007/s00382-006-0135-7.

Chauvin, F., Royer, J.F., Déqué, M., 2006b. Response of hurricane-type vortices to global warming as simulated by ARPEGE-Climat at high resolution. *Climate Dynamics* 27, 377–399. URL: <http://link.springer.com/10.1007/s00382-006-0135-7>, doi:doi:10.1007/s00382-006-0135-7.

CMCC, . High performance computing center – hpcc. <https://www.cmcc.it/what-we-do/high-performance-computing-center-hpcc>. Accessed: 2025-07-10.

Dabhade, A., Roy, S., Moustafa, M.S., Mohamed, S.A., El Gendy, R., Barma, S., 2021. Extreme weather event (cyclone) detection in india using advanced deep learning techniques, in: 2021 9th International Conference on Orange Technology (ICOT), pp. 1–4. doi:doi:10.1109/ICOT54518.2021.9680663.

Dee, D.P., Uppala, S.M., Simmons, A.J., Berrisford, P., Poli, P., Kobayashi, S., Andrae, U., Balmaseda, M.A., Balsamo, G., Bauer, P., Bechtold, P., Beljaars, A.C.M., van de Berg, L., Bidlot, J., Bormann, N., Delsol, C., Dragani, R., Fuentes, M., Geer, A.J., Haimberger, L., Healy, S.B., Hersbach, H., Hólm, E.V., Isaksen, L., Källberg, P., Köhler, M., Matricardi, M., McNally, A.P., Monge-Sanz, B.M., Morcrette, J.J., Park, B.K., Peubey, C., de Rosnay, P., Tavolato, C., Thépaut, J.N., Vitart, F., 2011. The era-interim reanalysis: configuration and performance of the data assimilation system. *Quarterly Journal of the Royal Meteorological Society* 137, 553–597. URL: <https://rmets.onlinelibrary.wiley.com/doi/abs/10.1002/qj.828>, doi:doi:<https://doi.org/10.1002/qj.828>, arXiv:<https://rmets.onlinelibrary.wiley.com/doi/pdf/10.1002/qj.828>.

Elsner, J.B., Kossin, J.P., Jagger, T.H., 2008. The increasing intensity of the strongest tropical cyclones. *Nature* 455, 92–95. URL: <https://doi.org/10.1038/nature07234>, doi:doi:10.1038/nature07234.

Emanuel, K., 2003. Tropical cyclones. *Annual Review of Earth and Planetary Sciences* 31, 75–104. URL: <https://doi.org/10.1146/annurev.earth.31.100901.141259>, doi:doi:10.1146/annurev.earth.31.100901.141259, arXiv:<https://doi.org/10.1146/annurev.earth.31.100901.141259>.

Emanuel, K.A., Nolan, D.S., 2004. Tropical cyclone activity and the global climate system, in: Preprints, 26th Conf. on Hurricanes and Tropical Meteorology, Miami, FL, Amer. Meteor. Soc. A.

Enz, B.M., Engelmann, J.P., Lohmann, U., 2022. Parallel use of threshold parameter variation for tropical cyclone tracking. *Geoscientific Model Development Discussions* 2022, 1–29. URL: <https://gmd.copernicus.org/preprints/gmd-2022-279/>, doi:doi:10.5194/gmd-2022-279.

Galea, D., Kunkel, J., Lawrence, B.N., 2023. TCDetect: A New Method of Detecting the Presence of Tropical Cyclones Using Deep Learning. *Artificial Intelligence for the Earth Systems* 2, e220045. URL: <https://journals.ametsoc.org/view/journals/aies/2/3/AIES-D-22-0045.1.xml>, doi:doi:10.1175/AIES-D-22-0045.1.

Garner, A.J., Kopp, R.E., Horton, B.P., 2021. Evolving tropical cyclone tracks in the north atlantic in a warming climate. *Earth's Future* 9, e2021EF002326. URL: <https://agupubs.onlinelibrary.wiley.com/doi/abs/10.1029/2021EF002326>, doi:doi:<https://doi.org/10.1029/2021EF002326>, arXiv:<https://agupubs.onlinelibrary.wiley.com/doi/pdf/10.1029/2021EF002326>. e2021EF002326 2021EF002326.

Gray, W.M., 1975. Tropical cyclone genesis. Ph.D. thesis. Colorado State University. Libraries.

Haque, M.N., Ashfaqul Adel, A.A.M., Alam, K.S., 2022. Deep learning techniques in cyclone detection with cyclone eye localization based on satellite images, in: Arefin, M.S., Kaiser, M.S., Bandyopadhyay, A., Ahad, M.A.R., Ray, K. (Eds.), Proceedings of the International Conference on Big Data, IoT, and Machine Learning, Springer Singapore, Singapore. pp. 461–472.

Hersbach, H., Bell, B., Berrisford, P., Biavati, G., Horányi, A., Muñoz Sabater, J., Nicolas, J., Peubey, C., Radu, R., Rozum, I., Schepers, D., Simmons, A., Soci, C., Dee, D., Thépaut, J.N., 2023. ERA5 hourly data on single levels from 1940 to present. Copernicus Climate Change Service (C3S) Climate Data Store (CDS) doi:doi:10.24381/cds.adbb2d47.

Hodges, K., Cobb, A., Vidale, P.L., 2017a. How well are tropical cyclones represented in reanalysis datasets? *Journal of Climate* 30, 5243 – 5264. URL: <https://journals.ametsoc.org/view/journals/clim/30/14/jcli-d-16-0557.1.xml>, doi:doi:<https://doi.org/10.1175/JCLI-D-16-0557.1>.

Hodges, K., Cobb, A., Vidale, P.L., 2017b. How Well Are Tropical Cyclones Represented in Reanalysis Datasets? *Journal of Climate* 30, 5243–5264. URL: <https://journals.ametsoc.org/doi/10.1175/JCLI-D-16-0557.1>, doi:doi:<https://doi.org/10.1175/JCLI-D-16-0557.1>.

Horn, M., Walsh, K., Zhao, M., Camargo, S.J., Scoccimarro, E., Murakami, H., Wang, H., Ballinger, A., Kumar, A., Shaevitz, D.A., Jonas, J.A., Oouchi, K., 2014. Tracking scheme dependence of simulated tropical cyclone response to idealized climate simulations. *Journal of Climate* 27, 9197 – 9213. URL: <https://journals.ametsoc.org/view/journals/clim/27/24/jcli-d-14-00200.1.xml>, doi:doi:<https://doi.org/10.1175/JCLI-D-14-00200.1>.

IBTrACS Science Team, 2019. International Best Track Archive for Climate Stewardship (IBTrACS) Technical Documentation. Technical Report. National Oceanic and Atmospheric Administration.

Kim, M., Park, M.S., Im, J., Park, S., Lee, M.I., 2019. Machine learning approaches for detecting tropical cyclone formation using satellite data. *Remote Sensing* 11. URL: <https://www.mdpi.com/2072-4292/11/10/1195>, doi:doi:[10.3390/rs11101195](https://doi.org/10.3390/rs11101195).

Knapp, K.R., Kruk, M.C., Levinson, D.H., Diamond, H.J., Neumann, C.J., 2010. The international best track archive for climate stewardship (ibtracs): Unifying tropical cyclone data. *Bulletin of the American Meteorological Society* 91, 363 – 376. URL: https://journals.ametsoc.org/view/journals/bams/91/3/2009bams2755_1.xml, doi:doi:<https://doi.org/10.1175/2009BAMS2755.1>.

Kumler-Bonfanti, C., Stewart, J., Hall, D., Govett, M., 2020. Tropical and extratropical cyclone detection using deep learning. *Journal of Applied Meteorology and Climatology* 59, 1971 – 1985. URL: <https://journals.ametsoc.org/view/journals/apme/59/12/jamc-d-20-0117.1.xml>, doi:doi:<https://doi.org/10.1175/JAMC-D-20-0117.1>.

Lam, L., George, M., Gardoll, S., Safieddine, S., Whitburn, S., Clerbaux, C., 2023. Tropical cyclone detection from the thermal infrared sensor iasi data using the deep learning model yolov3. *Atmosphere* 14. URL: <https://www.mdpi.com/2073-4433/14/2/215>, doi:doi:[10.3390/atmos14020215](https://doi.org/10.3390/atmos14020215).

Lecun, Y., Bottou, L., Bengio, Y., Haffner, P., 1998. Gradient-based learning applied to document recognition. *Proceedings of the IEEE* 86, 2278–2324. doi:doi:[10.1109/5.726791](https://doi.org/10.1109/5.726791).

Lin, X.J., Huang, G.H., Song, T.N., 2025. Enhanced Global Tropical Cyclone Identification in ERA5 Through Bayesian Inference and Dynamic Tracking (BIDTrack) Algorithm. *Journal of Climate* URL: <https://journals.ametsoc.org/view/journals/clim/aop/JCLI-D-24-0484.1/JCLI-D-24-0484.1.xml>, doi:doi:[10.1175/JCLI-D-24-0484.1](https://doi.org/10.1175/JCLI-D-24-0484.1).

Loshchilov, I., Hutter, F., 2019. Decoupled Weight Decay Regularization. URL: <http://arxiv.org/abs/1711.05101>, doi:doi:[10.48550/arXiv.1711.05101](https://arxiv.org/abs/1711.05101). arXiv:1711.05101 [cs].

Matsuoka, D., Nakano, M., Sugiyama, D., Uchida, S., 2018. Deep learning approach for detecting tropical cyclones and their precursors in the simulation by a cloud-resolving global nonhydrostatic atmospheric model. *Progress in Earth and Planetary Science* 5, 80. URL: <https://progearthplanetsci.springeropen.com/articles/10.1186/s40645-018-0245-y>, doi:doi:[10.1186/s40645-018-0245-y](https://doi.org/10.1186/s40645-018-0245-y).

Mendelsohn, R., Emanuel, K., Chonabayashi, S., Bakkenes, L., 2012. The impact of climate change on global tropical cyclone damage. *Nature Climate Change* 2, 205–209. URL: <https://doi.org/10.1038/nclimate1357>, doi:doi:[10.1038/nclimate1357](https://doi.org/10.1038/nclimate1357).

Mueller, T.J., Patricola, C.M., Bercos-Hickey, E., 2024. The influence of enso diversity on future atlantic tropical cyclone activity. *Journal of Climate* 37, 3959 – 3975. URL: <https://journals.ametsoc.org/view/journals/clim/37/15/JCLI-D-23-0286.1.xml>, doi:doi:[10.1175/JCLI-D-23-0286.1](https://doi.org/10.1175/JCLI-D-23-0286.1).

Murakami, H., 2014. Tropical cyclones in reanalysis data sets. *Geophysical Research Letters* 41, 2133–2141. URL: <https://agupubs.onlinelibrary.wiley.com/doi/abs/10.1002/2014GL059519>, doi:doi:<https://doi.org/10.1002/2014GL059519>. arXiv:<https://agupubs.onlinelibrary.wiley.com/doi/pdf/10.1002/2014GL059519>.

Nair, A., Srujan, K.S.S.S., Kulkarni, S.R., Alwadhi, K., Jain, N., Kodamana, H., Sandeep, S., John, V.O., 2022. A deep learning framework for the detection of tropical cyclones from satellite images. *IEEE Geoscience and Remote Sensing Letters* 19, 1–5. doi:doi:[10.1109/LGRS.2021.3131638](https://doi.org/10.1109/LGRS.2021.3131638).

Pang, S., Xie, P., Xu, D., Meng, F., Tao, X., Li, B., Li, Y., Song, T., 2021. Ndftc: A new detection framework of tropical cyclones from meteorological satellite images with deep transfer learning. *Remote Sensing* 13. URL: <https://www.mdpi.com/2072-4292/13/9/1860>, doi:doi:[10.3390/rs13091860](https://doi.org/10.3390/rs13091860).

Roy, C., Kovordányi, R., 2012. Tropical cyclone track forecasting techniques — a review. *Atmospheric Research* 104–105, 40–69. URL: <https://www.sciencedirect.com/science/article/pii/S0169809511002973>, doi:doi:<https://doi.org/10.1016/j.atmosres.2011.09.012>.

Scoccimarro, E., Fogli, P.G., Reed, K.A., Gualdi, S., Masina, S., Navarra, A., 2017. Tropical cyclone interaction with the ocean: The role of high-frequency (subdaily) coupled processes. *Journal of Climate* 30, 145–162. URL: <https://doi.org/10.1175/jcli-d-16-0292.1>, doi:doi:[10.1175/jcli-d-16-0292.1](https://doi.org/10.1175/jcli-d-16-0292.1).

Scoccimarro, E., Gualdi, S., Villarini, G., Vecchi, G.A., Zhao, M., Walsh, K., Navarra, A., 2014. Intense precipitation events associated with landfalling tropical cyclones in response to a warmer climate and increased co2. *Journal of Climate* 27, 4642 – 4654. URL: <https://journals.ametsoc.org/view/journals/clim/27/12/jcli-d-14-00065.1.xml>, doi:doi:<https://doi.org/10.1175/JCLI-D-14-00065.1>.

Shakya, S., Kumar, S., Goswami, M., 2020. Deep learning algorithm for satellite imaging based cyclone detection. *IEEE Journal of Selected Topics in Applied Earth Observations and Remote Sensing* 13, 827–839. doi:doi:[10.1109/JSTARS.2020.2970253](https://doi.org/10.1109/JSTARS.2020.2970253).

Simonyan, K., Zisserman, A., 2015. Very Deep Convolutional Networks for Large-Scale Image Recognition. URL: <http://arxiv.org/abs/1409.1556>, doi:doi:[10.48550/arXiv.1409.1556](https://doi.org/10.48550/arXiv.1409.1556). arXiv:[1409.1556](https://arxiv.org/abs/1409.1556) [cs].

Slocum, C.J., Razin, M.N., Knaff, J.A., Stow, J.P., 2022. Does ERA5 Mark a New Era for Resolving the Tropical Cyclone Environment? *Journal of Climate* 35, 7147–7164. URL: <https://journals.ametsoc.org/view/journals/clim/35/21/JCLI-D-22-0127.1.xml>, doi:doi:[10.1175/JCLI-D-22-0127.1](https://doi.org/10.1175/JCLI-D-22-0127.1).

Strachan, J., Vidale, P.L., Hodges, K., Roberts, M., Demory, M.E., 2013. Investigating global tropical cyclone activity with a hierarchy of agcms: The role of model resolution. *Journal of Climate* 26, 133 – 152. URL: <https://journals.ametsoc.org/view/journals/clim/26/1/jcli-d-12-00012.1.xml>, doi:doi:<https://doi.org/10.1175/JCLI-D-12-00012.1>.

Sun, Y., Zhong, Z., Li, T., Yi, L., Hu, Y., Wan, H., Chen, H., Liao, Q., Ma, C., Li, Q., 2017. Impact of Ocean Warming on Tropical Cyclone Size and Its Destructiveness. *Scientific Reports* 7, 8154. URL: <https://doi.org/10.1038/s41598-017-08533-6>, doi:doi:[10.1038/s41598-017-08533-6](https://doi.org/10.1038/s41598-017-08533-6).

Tory, K.J., Chand, S.S., Dare, R.A., McBride, J.L., 2013a. The development and assessment of a model-, grid-, and basin-independent tropical cyclone detection scheme. *Journal of Climate* 26, 5493–5507. URL: <https://doi.org/10.1175/jcli-d-12-00510.1>, doi:doi:[10.1175/jcli-d-12-00510.1](https://doi.org/10.1175/jcli-d-12-00510.1).

Tory, K.J., Dare, R.A., Davidson, N.E., McBride, J.L., Chand, S.S., 2013b. The importance of low-deformation vorticity in tropical cyclone formation. *Atmospheric Chemistry and Physics* 13, 2115–2132. URL: <https://acp.copernicus.org/articles/13/2115/2013/>, doi:doi:[10.5194/acp-13-2115-2013](https://doi.org/10.5194/acp-13-2115-2013).

Tropical Cyclone 1983 JWTC Report, 1983. 1983 annual tropical cyclone report. URL: <https://apps.dtic.mil/sti/tr/pdf/ADA137836.pdf>. accessed: 2025-07-01.

Tropical Cyclones 1993 NOAA report, 1993. Tropical cyclones 1993 noaa report. URL: https://www.nhc.noaa.gov/data/tcr/CP1993_Seasonal_TCR.pdf. accessed: 2025-07-01.

Tropical Cyclones 1994 NOAA report, 1994. Tropical cyclones 1994 noaa report. URL: https://www.nhc.noaa.gov/data/tcr/CP1994_Seasonal_TCR.pdf. accessed: 2025-07-01.

Tropical Cyclones 1997 NOAA report, 1997. Tropical cyclones 1997 noaa report. URL: https://www.nhc.noaa.gov/data/tcr/CP1997_Seasonal_TCR.pdf. accessed: 2025-07-01.

Tropical Cyclones 1999 NOAA report, 1999. Tropical cyclones 1999 noaa report. URL: https://www.nhc.noaa.gov/data/tcr/CP1999_Seasonal_TCR.pdf. accessed: 2025-07-01.

Ullrich, P.A., Zarzycki, C.M., McClenny, E.E., Pinheiro, M.C., Stansfield, A.M., Reed, K.A., 2021. TempestExtremes v2.1: a community framework for feature detection, tracking, and analysis in large datasets. *Geoscientific Model Development* 14, 5023–5048. URL: <https://gmd.copernicus.org/articles/14/5023/2021/>, doi:doi:10.5194/gmd-14-5023-2021.

Vaitinada Ayar, P., Bourdin, S., Faranda, D., Vrac, M., 2025. Ensemble Random Forest for Tropical Cyclone Tracking. URL: <https://egusphere.copernicus.org/preprints/2025/egusphere-2025-252/>, doi:doi:10.5194/egusphere-2025-252.

Veness, C., 2022. Calculate distance, bearing and more between latitude/longitude points. URL: <https://www.movable-type.co.uk/scripts/latlong.html>. accessed: 2025-07-10.

Wang, P., Wang, P., Wang, C., Yuan, Y., Wang, D., 2020. A center location algorithm for tropical cyclone in satellite infrared images. *IEEE Journal of Selected Topics in Applied Earth Observations and Remote Sensing* 13, 2161–2172. doi:doi:10.1109/JSTARS.2020.2995158.

Weaver, M.M., Garner, A.J., 2023. Varying genesis and landfall locations for north atlantic tropical cyclones in a warmer climate. *Scientific Reports* 13. URL: <https://doi.org/10.1038/s41598-023-31545-4>, doi:doi:10.1038/s41598-023-31545-4.

World Meteorological Organization, 2023. Tropical cyclones. URL: <https://public.wmo.int/en/our-mandate/focus-areas/natural-hazards-and-disaster-risk-reduction/tropical-cyclones>. accessed on May 16, 2023.

Xie, M., Li, Y., Cao, K., 2020. Global cyclone and anticyclone detection model based on remotely sensed wind field and deep learning. *Remote Sensing* 12. URL: <https://www.mdpi.com/2072-4292/12/19/3111>, doi:doi:10.3390/rs12193111.

Yan, L., Guo, H., Peterka, T., Wang, B., Wang, J., 2023. TROPHY: A Topologically Robust Physics-Informed Tracking Framework for Tropical Cyclones. URL: <http://arxiv.org/abs/2307.15243>, doi:doi:10.48550/arXiv.2307.15243. arXiv:2307.15243 [physics].

Zarzycki, C.M., Ullrich, P.A., 2017. Assessing sensitivities in algorithmic detection of tropical cyclones in climate data. *Geophysical Research Letters* 44, 1141–1149. URL: <https://doi.org/10.1002/2016gl071606>, doi:doi:10.1002/2016gl071606.

Zhang, Y., Sun, P., Jiang, Y., Yu, D., Weng, F., Yuan, Z., Luo, P., Liu, W., Wang, X., 2022. ByteTrack: Multi-Object Tracking by Associating Every Detection Box. URL: <http://arxiv.org/abs/2110.06864>, doi:doi:10.48550/arXiv.2110.06864. arXiv:2110.06864 [cs].

Zhao, M., Held, I.M., Lin, S.J., Vecchi, G.A., 2009. Simulations of global hurricane climatology, interannual variability, and response to global warming using a 50-km resolution GCM. *Journal of Climate* 22, 6653–6678. URL: <https://doi.org/10.1175/2009jcli3049.1>, doi:doi:10.1175/2009jcli3049.1.

A Appendix

A.1 Hyperparameter tuning of BYTE

To select the best configuration of data-driven models and BYTE-based tracking, an optimization algorithm was used. Specifically, fixing the bounding box size to 25, the *Track Buffer* to 1 and varying both the *Match* and *Track Threshold*, a first grid-search was performed. This preliminary operation aimed at finding the best candidates for *Match*- and *Track-Threshold* while, at the same time, avoiding the high computational cost of the grid search. Within the pool of candidates, the TC tracker having *Match Threshold* = 0.8 and *Track Threshold* = 0.7 was selected and referred to as the *Baseline*. Its skills are $POD = 84.2$, $FAR = 28.23$, $r_{ENP} = 0.63$ and $r_{WNP} = 0.71$. POD and FAR were computed on the joint ENP-WNP basins, considered as a whole.

The selection criteria adopted in this phase was to find out the model having a POD higher than TRACK one and a good trade-off between FAR , track duration and the Pearson correlation on ENP and WNP.

After this phase, the *Bounding Box Size* was then varied in the set $BB = \{15, 21, 25, 31, 35\}$ and the *Track Buffer* in $TB = \{1, 2, 3, 4\}$. Since the spatial resolution of the ERA5 climatic drivers is $0.25^\circ \times 0.25^\circ$, the bounding box size lower bound (15) and upper bound (35) were chosen in order to have physically meaningful DL-trackers, thus avoiding TC tracks with too far detections (i.e., above 400 km). On the other hand, the *Track Buffer* was set to a maximum of 4 time-steps, similarly to Ullrich et al. (2021) tracker. The total number of possible DL-Trackers was 20 in this phase.

The pool of candidates was augmented including some physical constraints: i) removing TCs originating on land, ii) removing TCs originating above 30° Latitude (Hodges et al. (2017b)) and iii) removing TCs originating above 50° Latitude (Ullrich et al. (2021)). In addition to the aforementioned 3 post-processing, the combination i)-ii) and i)-iii) were added. Therefore, a total of 120 different DL-trackers candidates was reached.

Among the resulting pool of DL-Trackers, the best Tracker was selected according to a simple weighted multi-objective optimization algorithm based on the Pareto Frontier. The targeted metrics to be optimized were POD , FAR , Pearson Correlation on ENP and WNP, whose assigned weights, w , were $w_{POD} = 0.4$, $w_{FAR} = 0.3$, $w_{ENP} = 0.15$, $w_{WNP} = 0.15$. The resulting DL-Tracker was the one with bounding box size equal to 21, excluding TCs originating above 30° Latitude, with skills: $POD = 82.25\%$, $FAR = 18.63\%$, $r_{ENP} = 0.75$ and $r_{WNP} = 0.69$. It was selected to be the ByteStorm tracker used in this work.

A.2 Additional results of ByteStorm

Aiming at assessing the skills of ByteStorm and extending the already provided results, we report additional details and results in this section. Specifically, we detailed the latitude-longitude distribution between IBTrACS observations and the predicted TC centers, as well as we provide additional details regarding the 5 longest TC tracks available in the test set.

A.2.1 Latitude and Longitude distribution

Regarding the localization accuracy, Figure A.1 shows the predicted and true Latitude (left panel) and Longitude (right panel) distributions over the Test Set (August 1980-2019). Red bisector line represents the theoretical perfect alignment between true and predicted TC geographical coordinates. The side color bar reports the MSW of the TCs matched between IBTrACS and ByteStorm. As can be seen in the image, longitudes are mostly distributed around the bisector line, while the lower latitudes have higher variability in terms of positional accuracy. Bytestorm is biased towards underestimating the real TC latitude, as the dots in Figure A.1 are mostly located above the red bisector. Additionally, it appears that stronger TCs (i.e., characterized by high MSW) report high positional precision, meaning that ByteStorm is accurate when the TCs are characterized by well-formed wind patterns.

A.2.2 Additional results on the 5 Longest TC Tracks

In this sub-section, after a brief description of the 5 longest TC tracks considered in this work, additional information is provided to better highlight the skills of the ByteStorm proposed in this work.

- **Tropical Cyclone Abby (1983):** Typhoon Abby is not considered one of the most dangerous or disruptive TCs ever historically occurred, however it aroused research community interest as most of the predicted tracks were 90° to the left of the actual TC track (Chan, 1986). It started on the 31st July 1983 as a small perturbation, and its development became relevant on the 7th August as it intensified rapidly. It then land-fell in Japan, causing several damages over a wide area, causing floods and landslides. It then weakened as it moved away from the land (Tropical Cyclone 1983 JWTC Report).

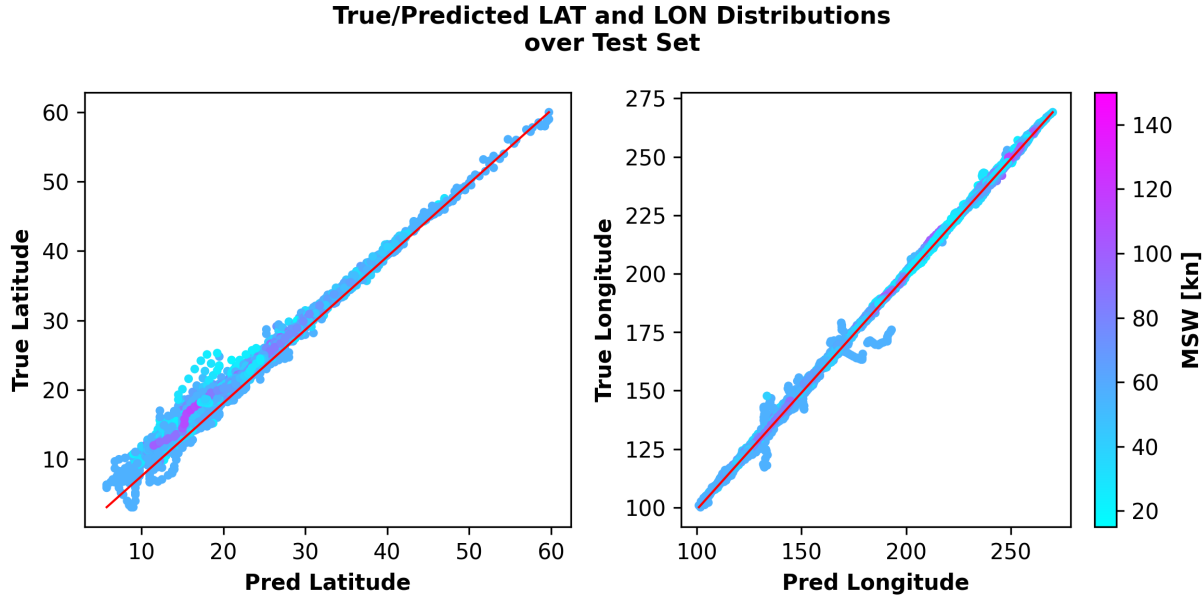


Figure A.1: Distribution of Predicted-True Latitudes (left) and Longitudes (right). Red bisector lines represent the perfect matching between predicted and true positions, while each colored dot represent the predicted TC eye position with respect to the correct one. The color of the dots represents the Maximum Sustained Wind of the TC observation.

- **Tropical Cyclone Keoni (1993):** Keoni's peak in wind intensity was recorded to 115 kn, and forced the evacuation of thousands of people from Johnston Atoll to Honolulu as the storm was moving towards the atoll. Keoni was considered a very compact and intense TC, as its powerful winds were circumscribed to a small area. As it moved away from Johnston Atoll, it weakened and slowed down. After it regained strength, it passed the north of Wake Island. Keoni's system was recorded as one of the longest-lived TCs in the Hawaiian islands (Tropical Cyclones 1993 NOAA report).
- **Tropical Cyclone John (1994):** TC John was considered one of the most intense Hurricanes ever recorded in the Central Pacific, as its MSW reached 150 kn. It caused several heavy rains phenomena and minor floodings over some islands in the Hawaii. The damage caused by the TC was estimated to about 15 million dollars (Tropical Cyclones 1994 NOAA report).
- **Tropical Cyclone Guillermo (1997):** It was developed as a disturbance near the coasts of Central America on July 29th. Then, it was classified as a Hurricane on the 1st of August continuously gaining energy, with estimated winds up to 140 kn. Some days after it quickly started weakening as it moved towards the central pacific. There, the TC gained energy, strengthening again. Finally, it weakened and de-classified as a disturbance as it moved back to the coasts of California. Only the Hawaii was affected by the swell caused by the winds peak (Tropical Cyclones 1997 NOAA report).
- **Tropical Cyclone Dora (1999):** Dora's cyclonic system during its lifetime originated about 300 miles south of Acapulco, in Mexico. As it moved west-ward it gained energy and was classified as a TS. It gained and lost energy as it moved during its path, causing small to no damages and light rain on Hawaii islands. The satellite imagery highlighted that Dora TC had a well developed TC eye (Tropical Cyclones 1999 NOAA report).

In Figure A.2 the 5 longest TC tracks are reported. Each TC tracker, as well as the IBTrACS ground truth (in red), are displayed during the TCs lifetime. To highlight the basins of MSLP minimum along the TC tracks, the sub-plots are overlaid on the minimum MSLP computed over all the 6-hourly time-steps belonging to the TC track. Aided by BYTE method, ByteStorm (in yellow) smoothly follows the historical observations for each of the considered cyclones. In contrast to other TC trackers such as CNRM (orange) and OWZ (purple), ByteStorm visually provides the smoothest tracks, as already explained in section 4.1.4. While TRACK Tracker (green) over-estimates the length of most of the TCs, our TC Tracker is closer to the real TC lifetime.

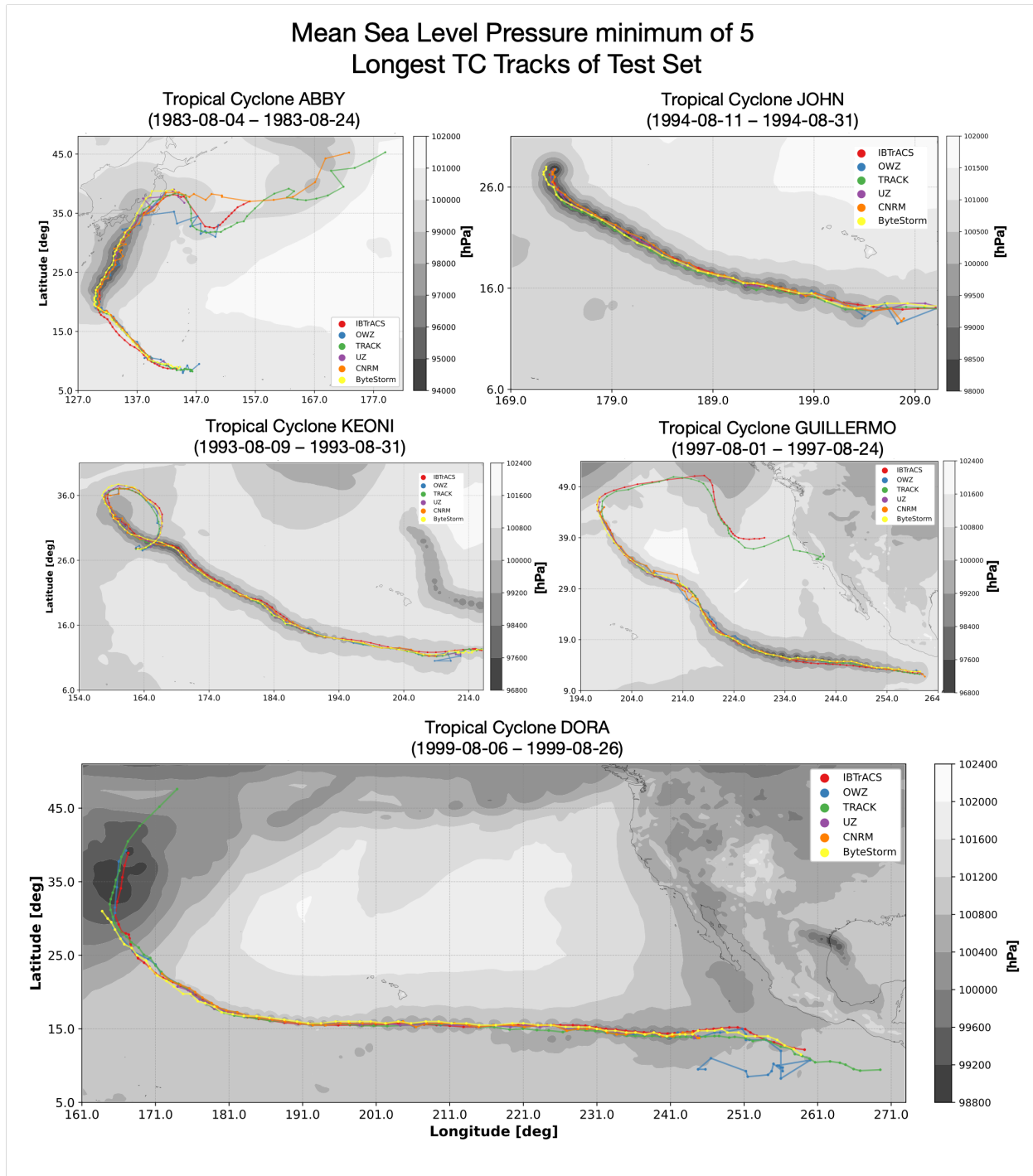


Figure A.2: IBTrACS (in red) and detected TC centers (other colors) of 5 longest TC tracks of the Test Set. The TCs reported in the figure, from left to right, top to bottom, are: Abby, John, Keoni, Guillermo and Dora. Detected TC Tracks are overlaid on the MSLP minimum computed over the entire TC track at 6-hourly time-steps, to highlight the local low-pressure basins.